# Probing Enantiospecific Interactions between Proline and an L-Glutathione Self-Assembled Monolayer by Modulation Excitation ATR-IR Spectroscopy

**Marco Bieri and Thomas Bürgi***

*Université de Neuchâtel, Institut de Chimie, Rue Emile-Argand 11, 2007- Neuchâtel, Switzerland*

*Received: January 11, 2005; In Final Form: March 18, 2005*

The interaction of proline with self-assembled monolayers (SAMs) of L-glutathione ($\gamma$-glu-cys-gly) on gold was investigated by a combination of attenuated total reflection (ATR-IR) infrared and modulation excitation spectroscopy (MES). The latter technique makes use of phase-sensitive detection of periodically varying signals and allows discrimination between species with different kinetics such as dissolved proline and adsorbed molecules. By applying a convection−diffusion model coupled to adsorption and desorption, it was possible to extract relative adsorption and desorption rates from the experimental data for the two enantiomers of proline, fully accounting for mass transport within the flow-through cell. The results show that, in particular, the desorption kinetics is different for the two enantiomers. Therefore, the L-glutathione SAM can discriminate between enantiomers, D-proline being stronger bound. The IR spectra reveal that upon interaction with proline the adsorbed L-glutathione is protonated at the gly part of the molecule, which, in the absence of proline, is bound to the gold surface as carboxylate. The observed protonation of adsorbed L-glutathione upon interaction with proline goes along with a structural change of the former, which seems to play an important role for enantiodiscrimination.

## Introduction

Chiral surfaces and interfaces have received considerable interest in recent years because of their importance in separation[1] and sensing[2,3] of enantiomers, their application in heterogeneous enantioselective catalysis[4,5] and their possibly decisive role for the origin of biochemical homochirality.[6,7] Cleavage of quartz or calcite, materials with chiral bulk structures, leads to surfaces that are naturally chiral. Similarly, cleavage of metals, which have achiral bulk structure, along certain high Miller index planes exposes naturally chiral terrace-step-king structures.[8,9] Chiral surfaces can also be created by anchoring or adsorption of a chiral molecule on a nonchiral surface.[10−15] In the latter case, the adsorption of the chiral molecule can even lead to supramolecular chiral assemblies, thus forming patterns that destroy the symmetry of the underlying surface.[11] In the absence of long-range ordering, the chirality of such surfaces is solely associated with the chirality of the adsorption complex.

The ability to differentiate between enantiomers of a chiral probe molecule is one of the most interesting properties of a chiral surface. It has, for example, been found that the enantiomers of glucose are electrooxidized at different rates on intrinsically chiral Pt(643) electrodes.[9] It has also been reported that (*R*)-3-methylcyclohexanone desorbs enantiospecifically from the two enantiomeric forms of the chiral Cu(643) surface[16] and that the enantiospecific desorption occurs from the chiral kink sites.[17] Examples of enantiodiscrimination of chirally modified surfaces are numerous and include, for example, the chiral stationary phases used in chromatography. Despite the numerous reports on enantiodiscriminating interfaces, not much molecular-level information is available on the relevant intermolecular interactions between surface (selector) and analyte molecule (selectand). This is because most of the applied experimental methods merely quantify enantiodiscrimination without giving direct molecular-level insight. For example, chromatographic methods derive separation factors from retention times. Other methods measure a mass change[18] or a change in the optical thickness due to adsorption.[2] Even further methods such as atomic force microscopy rely on force measurements between selector and selectand.[3] Other approaches make use of soluble model systems in order to investigate the relevant intermolecular interactions by applying bulk techniques.[19] However, the observed interactions in solution may still vary from the ones relevant at the corresponding interface.

An ideal method to probe enantiodiscriminating interactions at interfaces would combine (surface) sensitivity with selectivity for the chiral information. Whereas the former criterion is met by many powerful surface science tools,[20] the latter is an attribute of chiroptical techniques such as circular dichroism,[21] vibrational circular dichroism,[22] or Raman optical activity.[23] The combination of both attributes mentioned above is a real challenge. Nonlinear optical techniques may turn out to be powerful in probing chiral interfaces.[24]

Infrared spectroscopy is well-established for the study of surfaces and interfaces, and it has been used to investigate the interaction of enantiomers with chiral surfaces.[17,25] The technique has the disadvantage that nonspecific interactions also give rise to signals. Thus, the adsorption of enantiomers on a chiral surface may result in very similar spectra, the interesting differences being overlaid by much stronger signals from molecules that interact with the surface in a nonspecific manner. To overcome these problems, we have recently combined attenuated total reflection (ATR)-IR[26] with modulation excitation spectroscopy (MES)[27,28] to probe chiral discrimination at solid−liquid interfaces.[29,30] MES selectively reveals the periodically changing signals stimulated by the modulation of an external parameter. By periodically changing the absolute configuration of the probe molecule (absolute configuration modulation),

* Phone ++41 32 718 24 12. Fax ++41 32 718 25 11. E-mail: thomas.burgi@unine.ch.

**SCHEME 1: Structure of Proline (top) and**
**L-Glutathione (GSH, bottom)**
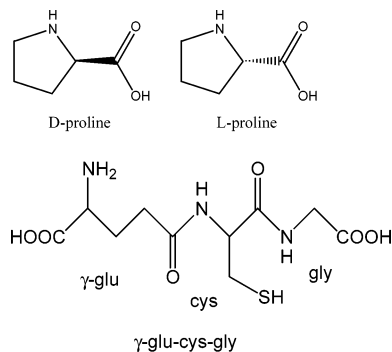


enantiospecific interactions can be spotted, as has been demonstrated for interactions taking place at chiral stationary phases.[29,30]

In the present work, we apply this strategy to investigate the interaction of proline with a chiral self-assembled monolayer (SAM) formed by adsorbing the tripeptide L-glutathione ($\gamma$-glu-cys-gly) on gold (see Scheme 1). L-Glutathione SAMs on electrodes revealed "ion gating" properties.[31,32] The interaction of cationic drugs, rare earth, and transition metal ions with the SAM leads to the opening of ion gates, as revealed by redox probes, and it has furthermore been proposed that the gating mechanism goes along with a conformational change of the adsorbed L-glutathione.[31,33] In a previous study, we reported on the reversible conformational changes within the L-glutathione SAM induced by acid and base stimuli.[34] It was furthermore shown that part of the adsorbed molecules interact with the gold surface, not only through the thiol but also through the carboxylic acid group of the gly moiety, which deprotonates upon adsorption.[34] The results presented below show that similar conformational changes are induced by the presence of the amino acid proline and that L-glutathione SAMs can differentiate between proline enantiomers.

**Experimental Section**

**Chemicals.** D- and L-Proline, respectively (Sigma-Aldrich, Inc., both >99%), were used as received. L-Glutathione ($\gamma$-glu-cys-gly, GSH, Sigma-Aldrich, Inc., ≥98%) was used without further purification. Ethanol (EtOH, Merck p.a.) was used as the solvent. Before each measurement, solutions were treated with nitrogen gas (99.995%, CarbaGas) to remove dissolved oxygen.

**In situ ATR-IR Spectroscopy.** *Sample Preparation.* The Ge internal reflection elements (IREs, 50 mm × 20 mm × 2 mm, 45°, Komlas) were polished with a 0.25-$\mu$m grain size diamond paste and rinsed copiously with EtOH. The surface was further plasma-cleaned under a flow of air for 5 min before a gold layer with a thickness of about 2 nm was sputtered onto the IRE. For each experiment, a fresh gold layer was used. Control experiments with the bare Ge IRE revealed no GSH adsorption as indicated by the absence of prominent GSH signals during several hours of exposure to GSH solution.

*Data Acquisition.* ATR-IR measurements were performed on a Bruker EQUINOX 55 FT-IR spectrometer equipped with a nitrogen-cooled narrow-band mercury cadmium telluride (MCT) detector. Spectra were recorded at a resolution of 4 cm$^{-1}$. A home-built liquid flow-through cell with a total volume of 0.077 mL and a gap of 250 $\mu$m between the IRE and the polished steel surface was used for ATR-IR experiments. The flow-
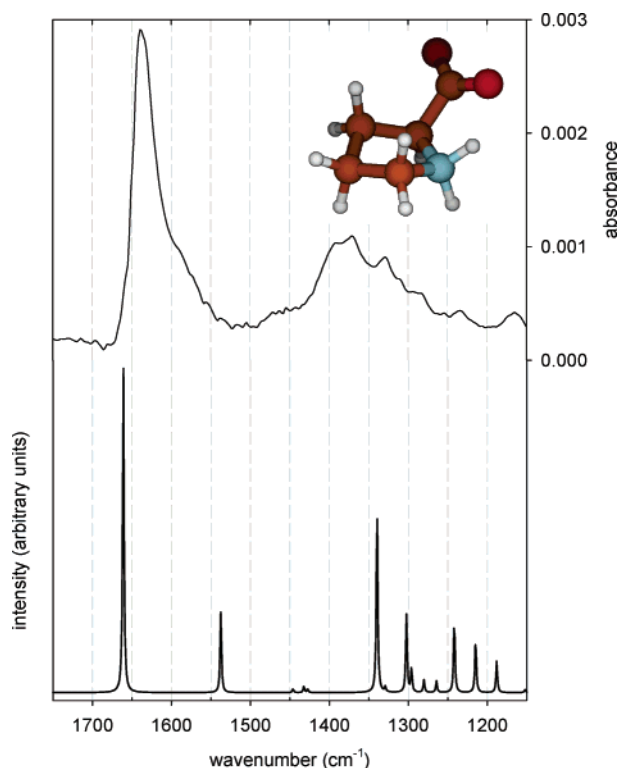
through cell can be heated or cooled, but all measurements reported here were performed at room temperature ($T = 298$ K). The ATR-IR cell is described in more detail elsewhere.[28,35]

*Modulation Experiments.* EtOH was used as the solvent for all ATR-IR measurements reported here. Before each experiment, the solvent was saturated with nitrogen gas (CarbaGas, 99.995%) and was flowed over the IRE until no variation in the spectrum could be detected (about 5 min). Then, a spectrum was recorded by coadding 200 interferograms which served as reference for all subsequent measurements. Several types of experiments were carried out: A first modulation experiment was performed by flowing periodically EtOH and L-proline over the bare and gold-coated Ge-IRE. This type of experiment yields the spectrum of dissolved proline and gives information about the interaction of proline with the bare gold surface. In a further experiment, GSH at typical concentrations of 0.33 mM was flowed over a freshly prepared gold surface. The adsorption process was stopped after 20 min and 4 h, respectively. The corresponding flow rates were 0.5 mL/min for 20 min and 0.18 mL/min for 4 h adsorption time. With these freshly prepared samples, modulation experiments were performed consisting of periodically flowing EtOH and D-proline over the GSH SAM. An analogous experiment was performed with L-proline at equal concentration. Information about the interaction of the corresponding enantiomer with the GSH SAM is obtained in these experiments. Finally, an absolute configuration modulation experiment was performed (i.e., the two enantiomers were allowed to flow alternately over the GSH SAM). A modulation period started with a flow of D-proline, followed by an equally long flow of L-proline over the GSH SAM. Probing enantiospecific interactions of proline with the GSH SAM is the goal of this experiment. All of the modulation experiments reported here consisted of two initial "dummy loops" to allow the system reaching a new quasi-stationary state followed by averaging over six measurement loops (periods). During one measurement period, 60 IR spectra were recorded at an 80 kHz sampling rate using the rapid scan acquisition mode of the Fourier transform (FT)-IR spectrometer. For each spectrum, 6 (30) interferograms per modulation period were averaged, resulting in a modulation period of $T = 72.4$ (362.3) s. By a subsequent digital phase sensitive detection (PSD) according to eq 1, phase-resolved spectra are obtained from the set of time-resolved spectra.

$$A_k^{\phi_k^{PSD}}(\tilde{\nu}) = \frac{2}{T} \int_0^T A(\tilde{\nu}, t) \sin(k\omega t + \phi_k^{PSD}) \, dt \qquad (1)$$

where $k = 1, 2, 3, \ldots$ determines the demodulation frequency (i.e., fundamental, first harmonic, and so on), $T$ is the modulation period, $\tilde{\nu}$ denotes the wavenumber, $\omega$ is the stimulation frequency and $\phi_k^{PSD}$ is the demodulation phase angle. With a set of time-resolved spectra $A(\tilde{\nu}, t)$, eq 1 can be evaluated for different phase angles $\phi_k^{PSD}$'s resulting in a series of phase-resolved spectra $A_k^{\phi_k^{PSD}}$. Only spectra demodulated at the fundamental frequency ($k = 1$) are reported here. A description in more detail of the modulation technique can be found elsewhere.[27,28]

**DFT Calculations of L-Glutathione and Proline.** To better understand the structure of GSH and proline and to assign the vibrational spectrum of proline, density functional theory (DFT) calculations were performed using the hybrid functional B3PW91[36,37] with a 6-31G basis set.[38] *GAUSSIAN 03* was used for all calculations.[39] Structures of GSH and proline are depicted in Scheme 1. A discussion of the results for the GSH DFT studies can be found elsewhere.[34] In case of proline, a

Enantiospecific Interaction of Proline with L-Glutathione SAM

*J. Phys. Chem. B, Vol. 109, No. 20, 2005* **10245**



**Figure 1.** Top: Demodulated spectrum of EtOH vs L-proline (0.044 M at a flow rate of 0.5 mL/min) modulation experiment on the bare Ge−IRE. Bottom: Calculated IR spectrum of proline after convolution with a Lorentzian band shape (half-width at half-maximum = 1 cm$^{-1}$). For details concerning the calculation method, see text.

polarizable continuum model (PCM)[40] was used to include the effect of the solvent. All calculations were performed with proline in zwitterionic form, as this prevails in ethanol. The conformation with lowest energy was found to have a hydrogen bond between the carboxylate and the protonated amine (see inset in Figure 1).

**Modeling Mass Transport and Surface Reactions.** To evaluate adsorption and desorption kinetics in a flow-through reactor, mass transport within the bulk phase has to be considered, which can conveniently be done using numerical methods. In a previous work, it was shown that mass transport of solute molecules within the ATR-IR flow-through cell can successfully be described by convection and diffusion using a simplified two-dimensional geometry.[35] The model used in the present work further couples adsorption, surface diffusion, and desorption to the transport of species to the surface. The following assumptions are made for the transport and adsorption model: (1) laminar flow of a (2) incompressible Newtonian fluid. (3) Because of the reduced two-dimensional geometry ($z$ denotes the direction perpendicular to the surface and $x$ the direction of the flow within the cell), there are no concentration variations in the $y$ direction and no velocity variations in the $x$ or $y$ direction. (4) Furthermore, interaction between solute molecules is neglected.

Steady-state momentum balance yields the following velocity profile which can be expressed in terms of the flow rate $\phi_V$.[41]

$$v_x(z) = \frac{6\phi_V}{wh^3}(hz - z^2) \qquad (2)$$

where $w$ is the width and $h$ the height of the simplified flow-through cell geometry.

Mass balance of solute species in the bulk is then given by the convection−diffusion equation

$$\frac{\partial c}{\partial t} = -v_x(z)\frac{\partial c}{\partial x} + D\left(\frac{\partial^2 c}{\partial x^2} + \frac{\partial^2 c}{\partial z^2}\right) \qquad (3)$$

The flux of the solute species in the bulk is expressed by

$$J = v_x(z)c - D\left(\frac{\partial c}{\partial x} + \frac{\partial c}{\partial z}\right) \qquad (4)$$

where $c$ denotes the bulk concentration of the solute molecule and $D$ is the diffusion coefficient.

On the surface boundary, the following reaction rate is defined

$$r_{\text{Surface}} = \frac{d\theta}{dt} = -k_{\text{ads}}c\theta + k_{\text{des}}c_S \qquad (5)$$

In eq 5, $\theta$ is the surface concentration of active sites, $c_s$ is the concentration of adsorbed molecules, and $k_{\text{ads}}$ and $k_{\text{des}}$ are the rate constants for adsorption and desorption, respectively. Note that the reaction rate expressed in eq 5 corresponds to a first-order Langmuir model. The first term on the right-hand side in eq 5, the surface concentration of active sites $\theta$, can be written as the difference between the total number of active sites $\theta_0$ and the surface concentration of adsorbed molecules $c_s$ according to

$$r_{\text{Surface}} = \frac{d\theta}{dt} = -k_{\text{ads}}c(\theta_0 - c_S) + k_{\text{des}}c_S \qquad (6)$$

The mass balance for the surface, including surface diffusion and the surface reaction rate as expressed in eq 6, is

$$\frac{\partial c_S}{\partial t} = D_S\frac{\partial^2 c_S}{\partial x^2} + k_{\text{ads}}c(\theta_0 - c_S) - k_{\text{des}}c_S \qquad (7)$$

where $D_s$ is the surface diffusion coefficient.

The following initial and boundary conditions were defined for the transport and adsorption model:

Initial conditions:

$$0 \leq x \leq L, 0 \leq z \leq h, c(t=0) = c_0, c_S(t=0) = 0 \quad (8)$$

where $L$ denotes the length between the inlet and outlet and $h$ the height of the cell. $C_0$ is the bulk concentration of the solute species.

Boundary conditions:

On the reactive surface (i.e., at $z = 0$), the boundary condition for the bulk couples the surface reaction rate with the flux of reacting species according to

$$J = v_x(z)c - D\left(\frac{\partial c}{\partial x} + \frac{\partial c}{\partial z}\right) = -k_{\text{ads}}c(\theta_0 - c_s) + k_{\text{des}}c_S \quad (9)$$

Other boundary conditions:

$$z = h, J = 0 \qquad (10)$$

$$\text{inlet } (x = 0), c = c_0 H(t) \qquad (11)$$

$$\text{outlet } (x = L), J = v_x(z)c \qquad (12)$$

In eq 11, the concentration modulation $H(t)$ is represented by a smoothed Heaviside function.

Simulations were performed using the finite element method (FEM) implemented in *FEMLAB*.[42] The transport and adsorption

model was solved using the real cell dimensions as $L = 36$ mm, $w = 7$ mm, and $h = 265$ $\mu$m. Furthermore, a flow rate of $\phi_V = 0.18$ mL/min and a concentration modulation ($c_0 = 4.3$ mM) frequency of 2.8 mHz were used. The total number of active sites $\theta_0$ was assumed to be $10^{15}$ molecules/cm$^2$. The diffusion coefficient $D$ of the solute species (proline in this case) was estimated according to the Stokes–Einstein equation

$$D = kT/(6\pi\eta a) \approx 3.7 \cdot 10^{-6} \text{ cm}^2/\text{s} \qquad (13)$$

where $\eta$ is the viscosity of the solvent and $a$ is the radius of the solute molecule approximated as a sphere. Note that the sphere radius of 5 Å of proline was derived from DFT calculations. The surface diffusion coefficient $D_s$ was further estimated to be 3 orders of magnitude smaller than the bulk diffusion coefficient $D$. Finally, $k_{ads}$ and $k_{des}$, respectively, are tunable parameters which were adjusted to fit the experimental curves. Note that experimentally available in an ATR-IR experiment are signals which are proportional to surface concentration $c_s$ and bulk concentration near the surface $c(z = 0)$. In an ATR-IR experiment, the signal is integrated over the internal reflection element. To compare with the experimental data, the concentrations were therefore averaged over $x$.

**Results**

A demodulated (phase-resolved) spectrum of the EtOH versus L-proline (0.044 M at a flow rate of 0.5 mL/min) modulation experiment on the bare Ge-IRE is depicted in Figure 1 (top). The spectrum reveals a prominent peak at 1637 cm$^{-1}$ with a shoulder at about 1570 cm$^{-1}$. In addition, a broad feature composed of several overlapping bands is visible in the region between 1400 and 1300 cm$^{-1}$. The calculated IR spectrum of proline is depicted in the bottom half of Figure 1. The spectrum was simulated by convoluting the calculated IR intensity with a Lorentzian band shape (half-width at half-maximum = 1 cm$^{-1}$). The calculated spectrum reveals a prominent signal at 1660 cm$^{-1}$ and a less intense band at 1537 cm$^{-1}$. A series of bands falls in the region between 1350 and 1200 cm$^{-1}$. Besides shifts in wavenumber, the overall agreement between calculated and measured spectra of proline in EtOH is good enough to allow assignment of the most prominent bands, as given in Table 1. The assignment is in line with previous reports.[43] Table 1 also contains assignments for the most relevant bands associated with GSH adsorbed on gold as reported previously.[34]

An ATR-IR spectrum of GSH adsorbed on gold is shown in Figure 2 (trace b). A spectrum recorded while flowing L-proline (0.044 M) over the GSH SAM is also shown in Figure 2 (trace a). The most prominent signals of GSH are visible at 1658 and 1535 cm$^{-1}$. Less intense bands are apparent at 1725 and 1400 cm$^{-1}$. The most intense L-proline band is visible at 1637 cm$^{-1}$ (compare to Figure 1). All other bands, namely the ones at 1725, 1540, and 1400 cm$^{-1}$, coincide well with the GSH signals already mentioned.

Figure 3 summarizes the phase-resolved spectra representing the interactions of each enantiomer (i.e., D- and L-proline, both at about 4.3 mM) with a GSH SAM after 20 min of self-assembling. The corresponding modulation experiment started with a flow of D- and L-proline, respectively, followed by an equal long flow of solvent (EtOH). Note that these spectra reveal only the signal that is periodically changing because of modulation of the proline concentration. Comparison between Figures 2 and 3 reveals important differences between demodulated and static spectra (Figure 2a). To study the time dependence of the adsorption/desorption of proline, modulation

**TABLE 1: Observed Vibrational Bands of GSH Adsorbed on Gold and Dissolved Proline (both in zwitterionic form) in EtOH[a]**

| GSH (zwitterionic) | proline (zwitterionic) | assignment |
|---|---|---|
| | static signals | |
| 1731 | | $\nu(-\text{COOH})$ |
| 1649 | | amide I |
| 1527 | | amide II |
| 1397 | | $\nu_s(-\text{COO}^-)$ |
| | phase-resolved signals | |
| | 1637 | $\nu_{as}(-\text{COO}^-)$ |
| | 1570 | $\delta_s(-\text{NH}_2)$ scissoring (appearing as shoulder of band at 1637 cm$^{-1}$) |
| | 1392 | $\nu_s(-\text{COO}^-) + \delta(-\text{CH})$ |
| | 1370 | $\nu_s(-\text{COO}^-) + \delta(-\text{CH})$ |
| | calculated signals | |
| | 1660 | $\nu_{as}(-\text{COO}^-)$ |
| | 1537 | $\delta_s(-\text{NH}_2)$ scissoring |
| | 1340 | $\nu_s(-\text{COO}^-) + \delta(-\text{CH})$ |
| | 1300 | $\nu_s(-\text{COO}^-) + \delta(-\text{CH})$ |

[a] The static GSH spectrum is depicted in Figure 2b and the phase-resolved proline spectrum is displayed in Figure 1 (top). Calculated proline vibrations are also included for comparison.
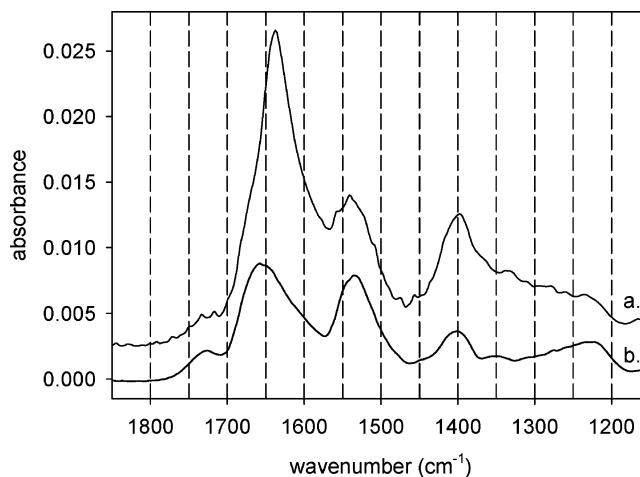


**Figure 2.** Static L-proline spectrum (trace a, 0.044 M) and GSH (trace b, 0.33 mM) spectrum after 5 min of adsorption. Note that the former spectrum was recorded while flowing L-proline over the GSH SAM (flow rate 0.5 mL/min) after 10 min onstream.

experiments with different modulation periods were performed, that is, $T = 72.4$ s (by coadding 6 interferograms, modulation experiment 1) and $T = 362.3$ s (by coadding 30 interferograms, modulation experiment 2). The flow rates were adjusted to the corresponding modulation periods to 0.5 mL/min ($T = 72.4$ s) and 0.18 mL/min ($T = 362.3$ s), respectively. Phase-resolved spectra of D-proline interaction with GSH SAM are depicted in the upper half of Figure 3 for modulation experiment 1 (trace b) and modulation experiment 2 (trace a), respectively. Obviously, the spectra differ considerably, indicating that the response to the described stimulation (D-proline concentration modulation) depends on the modulation frequency. This difference further reveals that species having different kinetics are observed in the spectra, such as dissolved proline and adsorbed molecules (proline and GSH). The phase-resolved spectrum of modulation experiment 1 reveals an intense asymmetric band at 1637 cm$^{-1}$ and a broad signal in the region between 1400 and 1300 cm$^{-1}$. This spectrum coincides well with the spectrum of dissolved proline (Figure 1). The phase-resolved spectrum of modulation experiment 2 (trace a in Figure 3) reveals signals
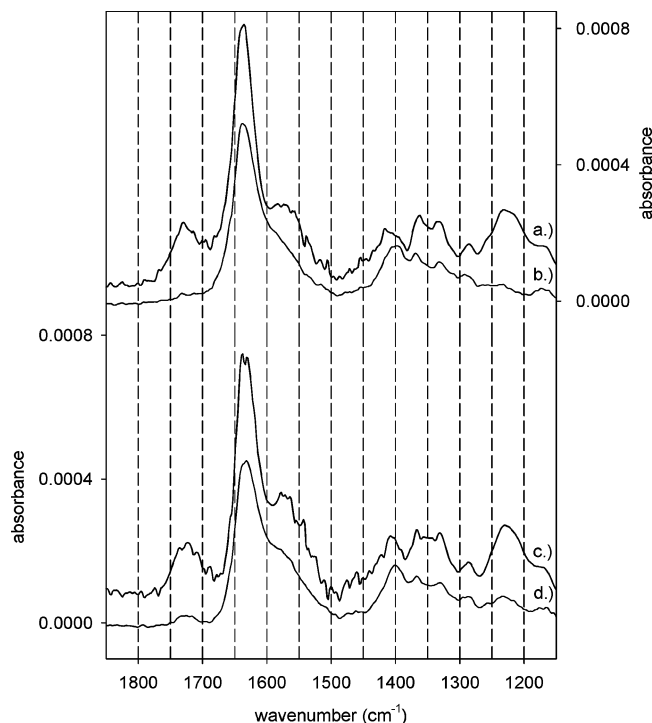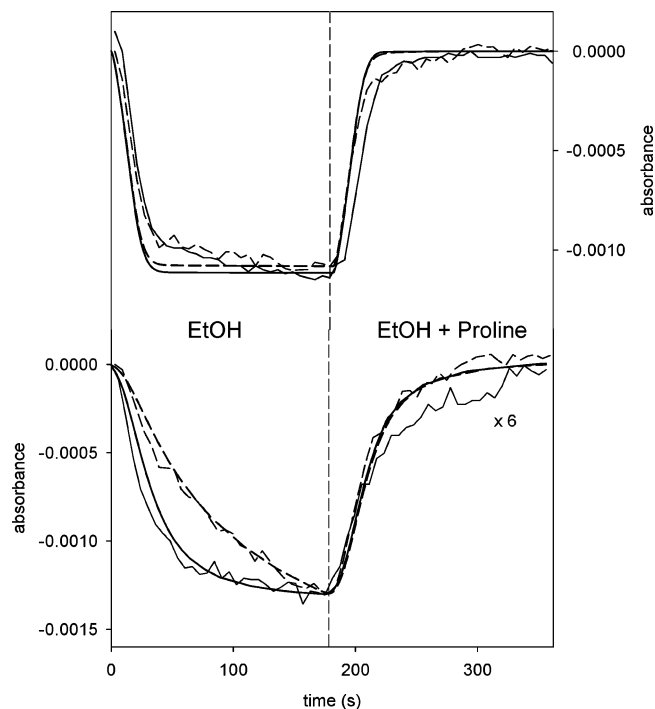
**Figure 3.** Phase-resolved spectra of EtOH vs D(L)-proline (both 4.3 mM) modulation experiment at different modulation frequencies (periods). Traces a and b refer to EtOH vs D-proline modulation experiment at $T = 72.4$ s (trace b) and $T = 362.3$ s (trace a) modulation periods. The same modulation experiments were performed for L-proline. Trace c refers to a modulation period of $T = 362.3$ s and trace d to $T = 72.4$ s. Note that flow rates were adjusted to the different modulation periods and amounted to 0.5 mL/min for $T = 72.4$ s and 0.18 mL/min for $T = 362.3$ s.



**Figure 4.** Time dependence of signals at 1625 (upper half in Figure 4) and 1725 cm$^{-1}$ (lower half in Figure 4) of the corresponding EtOH vs D(L)-proline modulation experiments performed at a modulation period of $T = 362.3$ s (note that the corresponding spectra are depicted in Figure 3, traces a and c). Dashed lines refer to D-proline and solid lines to L-proline. A typical modulation period started with a flow of EtOH (at 0.18 mL/min) over the GSH SAM (after 20 min of adsorption) indicated by "EtOH" in the left part of Figure 4. During the second half-period of the modulation experiment, EtOH was replaced by an equally long flow of D(L)-proline (dissolved in EtOH) indicated by "EtOH + proline" in the right part of Figure 4. The calculated time dependence of the signals using the transport and adsorption model is depicted by bold lines. Again, dashed lines refer to D-proline and solid lines to L-proline. Note that the signals in the upper half of Figure 4 refer to changes in the concentration of dissolved proline, whereas the signals in the lower half reflect variations in the surface concentration of proline due to adsorption/desorption on/from the GSH SAM.

at 1729 and 1637 cm$^{-1}$, whereas the former is hardly apparent in the case of modulation experiment 1. The band at 1637 cm$^{-1}$ further reveals a different band shape with a shoulder appearing at approximately 1570 cm$^{-1}$. Differences in intensity and position of the broad band in the region between 1400 and 1300 cm$^{-1}$ are apparent; the band at 1400 cm$^{-1}$ is shifted to 1415 cm$^{-1}$, and the signal at approximately 1225 cm$^{-1}$ is clearly more intense in experiment 2.

The phase-resolved spectra of the EtOH versus L-proline modulation experiment are depicted in the lower half in Figure 3. The spectrum at the bottom (trace d) is the response to modulation experiment 1, whereas the spectrum above (trace c) corresponds to modulation experiment 2. Again, the two spectra differ significantly and in a similar manner as described above for D-proline (compare to the two spectra, traces a and b, in the upper half of Figure 3). Careful inspection yet reveals small differences between the spectra of the D- and L-proline interactions with the GSH SAM. It should be noted that the experiments with the two enantiomers were performed at different days on different samples. Also, the apparent larger noise in spectra a and c is due to a larger interference of gas-phase water in these experiments. Because the interaction of each enantiomer with the GSH SAM has been found to depend on modulation frequency, it is helpful to turn to the time dependence of selected signals in order to learn more about adsorption and desorption kinetics, respectively.

The time dependence of the signals at 1625 and 1725 cm$^{-1}$, respectively, for D- and L-proline, respectively, versus EtOH modulation experiment 2 ($T = 362.3$ s, coaddition of 30 interferograms) is displayed in Figure 4. Dashed lines refer to D-proline and solid lines to L-proline. In the upper half of Figure

4, the time dependence of the absorbance at 1625 cm$^{-1}$ is displayed for D- and L-proline, respectively, revealing no large differences. The dominant contribution to this signal stems from proline in solution, and a weaker signal from proline interacting with the GSH SAM is thus probably hidden. In other words, the time dependence of the 1625 cm$^{-1}$ signal mainly originates from changes in the concentration of dissolved proline forced by convection and diffusion. On the other hand, the time dependence of the signal at approximately 1725 cm$^{-1}$ shows significant differences between D- and L-proline. During the first half-period of modulation experiment 2 (left part in the plot, indicated by "EtOH"), the flow of proline over the GSH SAM is replaced by EtOH, and the corresponding signals decrease with significantly different rates for the D- and L-proline experiments. Obviously, the decrease of the signal at 1725 cm$^{-1}$ is faster for the L-proline experiment and reaches steady state, whereas for the D-proline experiment the corresponding signal is still about to decrease after the first half-period of modulation experiment 2. During the second half-period of modulation, EtOH is replaced by dissolved proline (right part in the plot, indicated by "EtOH + proline"), which leads to an increase of the signal at 1725 cm$^{-1}$. In the D-proline experiment, the signal increases slightly more rapidly with time, almost reaching steady state at the end of the second half-period of modulation experiment 2. As will be shown later, the signal at about 1725

cm$^{-1}$ is likely associated with adsorbed GSH. Still, its appearance and disappearance are due to the interaction of proline with the GSH SAM and are therefore directly related to the adsorption/desorption kinetics. In summary, the signals at 1625 and 1725 cm$^{-1}$ belong to completely different system responses. The former signal refers to changes in the concentration of dissolved proline near the interface, whereas the latter reflects the surface concentration of proline due to adsorption/desorption on/from the GSH SAM. Assuming adsorption and desorption to be first-order reactions and absorbance to be proportional to concentration (Lambert−Beer law), the time dependence of signals depicted in Figure 4 was simulated using the transport and adsorption/desorption model described in the Experimental Section. The tunable parameters $k_{ads}$ and $k_{des}$ were adjusted to fit the experimental curves. The result of the corresponding simulations is depicted in Figure 4 as bold lines. Again, dashed lines refer to D-proline and solid lines to L-proline.

Obviously, the simulations represent the significant differences between the responses of the bulk (upper half in Figure 4) and surface (lower half in Figure 4) well. However, deviations from experimental data are visible, which may be explained by small volumes in the ATR-IR cell (behind inlet and outlet), where the fluid is almost stagnating,[35] and slight signal drifts during measurement. In addition, larger deviations between experimental and model data are apparent in the right lower half of Figure 4. The corresponding signals are related to the adsorption of D- and L-proline, respectively. Because the applied adsorption/desorption model assumes simple Langmuir kinetics, the observed discrepancy may indicate a more complex adsorption process that is not completely captured by the model. Knowing the adsorption and desorption rate constants allows calculating $\Delta\Delta G°$ of adsorption for D- and L-proline according to

$$\Delta\Delta G^0 = -RT \ln\left(\frac{K_D}{K_L}\right) \qquad (14)$$

where $K_{D,L} = k_{ads(D,L)}/k_{des(D,L)}$ denote the corresponding equilibrium constants of D- and L-proline, respectively. Evaluating eq 14 for $T = 298$ K, we found $K_D/K_L = 7.5$, and thus, $\Delta\Delta G° \approx -5.0$ kJ mol$^{-1}$. In other words, the GSH SAM seems to discriminate between D- and L-proline, with the former being more strongly bound. It should be pointed out that the derived value for $\Delta\Delta G°$ should be regarded as an order-of-magnitude estimate rather than an exact value, as its derivation relies on the kinetic model outlined above. Because the GSH SAM seems to distinguish between the proline enantiomers, signals can be expected for the absolute configuration modulation experiment when the two enantiomers (at 0.045 M) are allowed to flow alternately over the GSH SAM. A phase-resolved spectrum of such an experiment is depicted in Figure 5 (trace a, scaled by a factor of 25). The phase-resolved spectrum of the enantiospecific modulation experiment reveals a negative band at 1725 cm$^{-1}$ and a positive one at 1615 cm$^{-1}$. Furthermore, a broad positive band in the region between 1400 and 1250 cm$^{-1}$ is visible and a negative band at approximately 1225 cm$^{-1}$. The discussed spectrum is in good agreement with the one in the middle of Figure 5 (trace b, scaled by a factor of 25), which corresponds to the EtOH versus D-proline modulation experiment discussed above. By using one of the benefits of the modulation technique, namely the separation of species with different kinetics by choosing the phase angle $\phi_k^{PSD}$ in eq 1 accordingly, the contribution of dissolved proline was removed by adjusting $\phi_k^{PSD}$ such that the signal at 1637 cm$^{-1}$ vanished.
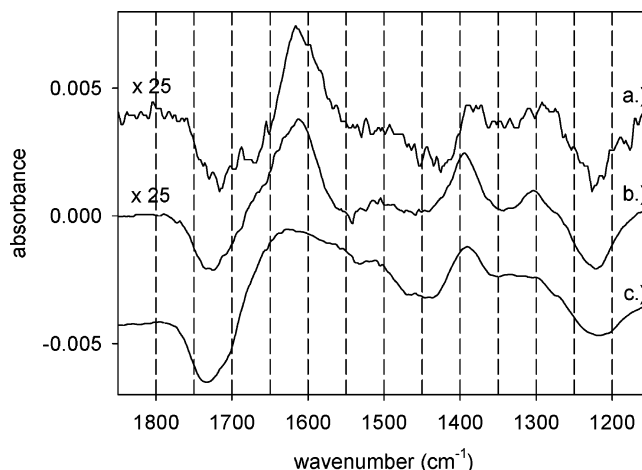


**Figure 5.** A demodulated ATR-IR spectrum of an absolute configuration modulation experiment (D- vs L-proline) is represented by trace a. The modulation experiment started with a flow of D-proline followed by an equally long flow of L-proline over the GSH SAM. The EtOH vs D-proline modulation experiment is displayed in trace b. The contribution from dissolved proline was minimized by choosing the demodulation phase angle accordingly. Trace c refers to an EtOH vs HCl (0.013 mM) in EtOH modulation experiment. In this kind of experiment, EtOH was allowed to flow over a GSH SAM (after 4 h of adsorption) during the first half-period and was replaced by acidic EtOH (HCl in EtOH) during the second half-period of the modulation experiment. The spectrum is a difference spectrum and represents the spectral changes during deprotonation in ethanol in the time interval between 50 and 241.6 s after switching to ethanol flow. This modulation experiment is described in more detail elsewhere.[34]

Obviously, the two spectra discussed above (traces a and b) are in good agreement with the bottom spectrum in Figure 5 (trace c). Trace c reveals an ATR-IR spectrum of another modulation experiment. In this experiment, neutral EtOH and HCl (0.013 mM) in EtOH was allowed to flow alternately over a GSH SAM after 4 h of adsorption. It was shown that GSH reversibly changes ionic form from zwitterionic to protonated state upon this stimulation. Further information about this kind of modulation experiment can be found elsewhere.[34]

## Discussion

The admittance of dissolved proline to GSH self-assembled onto gold leads to characteristic signals in the ATR-IR spectra. Some of the signals arise because of dissolved proline itself, notably the prominent band at 1637 cm$^{-1}$ ($\nu_{as}(COO^-)$). Other signals are not associated with dissolved proline, as the comparison between the spectra in Figure 1 (proline dissolved in ethanol) and Figure 3 (proline admitted to GSH SAM) shows. The latter signals are assigned to adsorbed species. A control experiment where proline was admitted to a bare gold surface revealed that the signals in Figure 3 do not arise from proline directly adsorbed on gold.

As can be seen in Figure 4, the signals from dissolved proline and the signals arising from adsorbed species have different kinetics of appearance and disappearance in the modulation experiments. As a consequence, their spectral contributions can be separated in the demodulated spectra by appropriately choosing the demodulation phase angle $\phi_k^{PSD}$, as was done in Figure 5. Note that the choice of $\phi_k^{PSD}$ in order to remove the signals of one species from the spectra is somewhat arbitrary when all the signals associated with that species are overlapping with signals from other species. This situation may apply in the present case. We chose the demodulation phase angle $\phi_k^{PSD}$ such that the prominent signal at 1637 cm$^{-1}$ vanished.

Enantiospecific Interaction of Proline with L-Glutathione SAM

*J. Phys. Chem. B, Vol. 109, No. 20, 2005* **10249**

The spectra associated with the adsorbed species in Figure 5 are characterized by negative bands at 1731 cm$^{-1}$ ($\nu$(C=O) of COOH) and 1222 cm$^{-1}$ ($\delta$(C−O−H) + $\nu$(C−O of COOH) and positive bands at 1615 cm$^{-1}$ ($\nu_{as}$(COO$^-$)), 1396 cm$^{-1}$ ($\nu_{sym}$(COO$^-$)), and 1303 cm$^{-1}$. Note that whether a band is positive or negative in a demodulated spectrum depends on the demodulation phase angle. For demodulation phase angles differing by 180°, the resulting spectra are inverted (positive bands become negative and vice versa) but otherwise identical. The spectral changes discussed above are characteristic of deprotonation/protonation of carboxylic acid groups. Figure 4 furthermore shows that the $\nu$(C=O) signal of the acid group (COOH) increases upon admitting proline, revealing that protonation of an acid group is taking place, and deprotonation occurs upon removal of proline.

Three carboxylic acid groups are involved in the system under consideration, two on GSH and one on proline. In ethanol, proline exists in zwitterionic form, as clearly shown by the ATR-IR spectra of the dissolved species (Figure 1), hence the acid is deprotonated (p$K_a$ = 1.99). GSH itself also exists in zwitterionic form in ethanol with the acid group on the glu part of the molecule deprotonated and the one on the gly part protonated.[34] However, we have shown recently that, upon adsorption of GSH onto gold, part of the molecules undergo deprotonation of the acid group of the gly moiety. This deprotonation is assisted by the interaction of the carboxylate group with the gold surface. Figure 5 shows that the demodulated spectrum obtained by modulating the proline concentration is very similar to a difference spectrum characteristic of deprotonation of the GSH sample in ethanol after admitting HCl. This strongly indicates that what is mainly seen in the demodulated spectra is the response of the GSH layer, which is partly protonated upon admission of proline and deprotonated during the subsequent ethanol flow. On the basis of previous work on GSH SAMs, we can even be more specific.[34] It was shown previously that the deprotonation of GSH in ethanol after protonation with HCl proceeds in two steps with distinctly different kinetics and spectral changes associated with them. A fast deprotonation of the glu part of the molecule is followed by a considerably slower deprotonation of the gly part. The latter step goes along with an interaction of the corresponding carboxylate group with the gold surface. Comparison shows that the spectral changes induced by the proline concentration modulation are similar to the ones observed during the deprotonation of the gly part of the molecule, in particular, the pronounced $\nu_{sym}$(COO$^-$) at 1396 cm$^{-1}$ is characteristic. The spectral changes thus indicate that, upon admitting proline, a fraction of the adsorbed GSH molecules are protonated at the gly moiety. Because proline exists as a zwitterion in ethanol (COO$^-$ and NH$_2^+$) a direct proton transfer from proline to GSH seems unlikely (p$K_a$(NH$_2^+$) = 10.60). We therefore propose that the surface is involved in the protonation process.

As shown in a previous study, in ethanol, a fraction of GSH adsorbed on gold is protonated at the gly moiety, and another fraction is deprotonated.[34] Changing the stability of either one of the two states involved in the equilibrium between protonated and deprotonated acid groups (bound to the surface) will shift the equilibrium. We therefore propose that the presence of proline at the interface stabilizes the protonated (not surface bound) state of the gly moiety of GSH through intermolecular interactions. The differences between the spectra in Figure 5 obtained when GSH is interacting with HCl and proline, respectively, in the spectral range between 1500 and 1600 cm$^{-1}$ may indicate such interactions.

The question that remains is why the spectra in Figure 5 mainly show the signatures of GSH, despite the fact that these changes are induced by the presence of proline at the interface. One possible explanation is based on the different sensitivity of the method for the two molecules. It has been reported that IR absorption is enhanced in the vicinity of metal and particularly gold films.[44] As one enhancement mechanism, a charge transfer has been proposed.[45] This mechanism differentiates between ions directly chemisorbed on the metal, for which a large enhancement is expected, and molecules weakly bound to the surface. This could explain why preferentially GSH signals are observed in the spectra. However, we prefer another interpretation. If the spectrum of proline interacting with the GSH SAM does not change much with respect to the spectrum of dissolved proline, as is expected in the absence of protonation/deprotonation of the molecule, then a differentiation between the two species is difficult. In this case, the contribution from the adsorbed proline is also subtracted when choosing the demodulation phase angle such that the contribution from the bulk (e.g., the strong $\nu_{as}$(COO$^-$) band at 1637 cm$^{-1}$) vanishes. At this point, it should be noted that, even if the vibrational frequencies of adsorbed and dissolved proline are the same, the relative band intensities could change upon adsorption, because the latter depend on the orientation of the molecule on the surface. The finding that preferentially GSH signals are observed in the demodulated spectra in Figure 5 thus indicates that the proline is either not strongly oriented on the surface, which seems unlikely, or that the orientation is such that the relative intensities of the most prominent bands of the adsorbed species are similar to the ones found in solution.

The spectra do not provide much insight concerning the exact nature of the intermolecular interaction between the GSH SAM and proline. From the demodulated spectra in Figure 5 and on the basis of a previous investigation,[34] it emerges that the protonation/deprotonation of adsorbed GSH upon adsorption/desorption of proline goes along with prominent structural changes within the GSH layer. The latter change may be similar to the ion gating observed when admitting cationic drugs or metal ions to GSH SAMs.[31,32]

Finally and most importantly, the experiments reveal that the GSH SAM differentiates between D- and L-proline, the former being more strongly bound. We have found that this enantiodifferentiation depends on the structure of the GSH SAM. SAMs that were assembled for 4 h instead of only 20 min did not show appreciable signals in the absolute configuration modulation experiments. We interpret this finding with the structural changes within the GSH SAM that go along with the interaction with proline. These changes may not be possible in a SAM that was assembled for a long time. Similarly, it was observed before that the structure of the SAM strongly depends on the conditions during adsorption of GSH (i.e., presence and absence of acid and base) and that this has a significant effect on the amplitude of the response toward acid stimuli.[34]

## Conclusions

L-Glutathione self-assembled on gold is found to discriminate between enantiomers of proline, with D-proline being the more strongly bound. The enantiodiscrimination was revealed by two independent types of experiments based on ATR-IR and modulation excitation spectroscopy. For the first, the adsorption/desorption kinetics of the two molecules was studied. To extract relative adsorption and desorption rates for the two enantiomers from the experimental curves, numeric simulations were performed, which couple mass transport (convection and diffusion)

Bieri and Bürgi

with adsorption and desorption. The ATR-IR experiments revealed that, in particular, the desorption kinetics is different for the two enantiomers. The numerical simulations reproduced the measured response associated with dissolved and adsorbed species toward concentration modulation well. Absolute configuration modulation excitation experiments further confirmed enantiodiscrimination. In the latter experiment, the absolute configuration of proline was changed periodically. The signals in the demodulated spectra reveal the difference in interaction of the two enantiomers with the chiral L-glutathione SAM.

Demodulated ATR-IR spectra associated with adsorbed species strongly resemble the spectral changes observed when changing the protonation state of L-glutathione adsorbed on gold. It could furthermore be concluded that the interaction of proline with adsorbed L-glutathione leads to protonation of the gly moiety of the latter. This process is reversible in the absence of proline in solution. In the absence of dissolved proline, part of the L-glutathione is deprotonated, and the carboxylate group of the gly part of the molecule interacts with the gold surface. The protonation of L-glutathione goes along with a significant structural change.

When the L-glutathione layer was allowed to self-assemble for a long time (4 h instead of 20 min) the enantiodiscrimination was virtually lost. This is explained by the structural change of L-glutathione upon interaction with proline, which may depend on the structure of the SAM. A similar dependence of the protonation/deprotonation response on the structure of the SAM was reported earlier. This indicates that enantiodiscrimination in this system is mainly associated with defects in the L-glutathione SAM.

## References and Notes

(1) Ahuja, S. *Chiral separations by chromatography*; Oxford University Press: Washington, DC, 2000.

(2) Bodenhöfer, K.; Hierlemann, A.; Seemann, J.; Gauglitz, G.; Koppenhoefer, B.; Göpel, W. *Nature (London)* **1997**, *387*, 577.

(3) McKendry, R.; Theoclitou, M.-E.; Rayment, T.; Abell, C. *Nature (London)* **1998**, *391*, 566.

(4) Bürgi, T.; Baiker, A. *Acc. Chem. Res.* **2004**, *37*, 909.

(5) Baiker, A.; Blaser, H. U. Enantioselective Catalysts and Reactions. In *Handbook of Heterogeneous Catalysis*; Ertl, G., Knözinger, H., Weitkamp, J., Eds.; VCH Publishers: Weinheim, 1997; Vol. 5, p 2422.

(6) Hazen, R. M.; Filley, T. R.; Goodfriend, G. A. *Proc. Natl. Acad. Sci. U.S.A.* **2001**, *98*, 5487.

(7) Zaia, D. A. M. *Amino Acids* **2004**, *27*, 113.

(8) McFadden, C. F.; Cremer, P. S.; Gellman, A. J. *Langmuir* **1996**, *12*, 2483.

(9) Attard, G. A. *J. Phys. Chem. B* **2001**, *105*, 3158.

(10) Lorenzo, M. O.; Haq, S.; Bertrams, T.; Murray, P.; Raval, R.; Baddeley, C. J. *J. Phys. Chem. B* **1999**, *103*, 10661.

(11) Lorenzo, M. O.; Baddeley, C. J.; Muryn, C.; Raval, R. *Nature (London)* **2000**, *404*, 376.

(12) Ferri, D.; Bürgi, T. *J. Am. Chem. Soc.* **2001**, *123*, 12074.

(13) Schunack, M.; Laegsgaard, E.; Steengaard, I.; Johannsen, I.; Besenbacher, F. *Angew. Chem, Int. Ed.* **2001**, *40*, 2623.

(14) Kühnle, A.; Linderoth, T. R.; Hammer, B.; Besenbacher, F. *Nature (London)* **2002**, *415*, 891.

(15) Ernst, K.-H.; Kuster, Y.; Fasel, R.; Müller, M.; Ellerbeck, U. *Chirality* **2001**, *13*, 675.

(16) Horvath, J. D.; Gellman, A. J. *J. Am. Chem. Soc.* **2002**, *124*, 2384.

(17) Horvath, J. D.; Koritnik, A.; Kamakoti, P.; Sholl, D. S.; Gellman, A. J. *J. Am. Chem. Soc.* **2004**, *126*, 14988.

(18) Nakanishi, T.; Yamakawa, N.; Asahi, T.; Osaka, T.; Ohtani, B.; Uosaki, K. *J. Am. Chem. Soc.* **2002**, *124*, 740.

(19) Maier, N. M.; Schefzick, S.; Lombardo, G. M.; Feliz, M.; Rissanen, K.; Lindner, W.; Lipkowitz, K. B. *J. Am. Chem. Soc.* **2002**, *124*, 8611.

(20) O'Conner, D. J.; Sexton, B. A.; Smart, R. S. C. *Surface analysis methods in materials science*; Springer series in surface science; Springer-Verlag: Berlin, 1992; Vol. 23.

(21) Alder, A. J.; Greenfield, N. J.; Fasman, G. D. *Methods Enzymol.* **1973**, *27*, 675.

(22) Nafie, L. A. *Annu. Rev. Phys. Chem.* **1997**, *48*, 357.

(23) Hug, W.; Kint, S.; Bailey, G. F.; Scherer, J. R. *J. Am. Chem. Soc.* **1975**, *97*, 5589.

(24) Hicks, J. M.; Petralli-Mallow, T. *Appl. Phys. B−* **1999**, *68*, 589.

(25) Gellman, A. J.; Horvath, J. D.; Buelow, M. T. *J. Mol. Catal A: Chem.* **2001**, *167*, 3.

(26) Harrick, N. J. *Internal reflection spectroscopy*; Interscience Publishers: New York, 1967.

(27) Baurecht, D.; Fringeli, U. P. *Rev. Sci. Instr.* **2001**, *72*, 3782.

(28) Bürgi, T.; Baiker, A. *J. Phys. Chem. B* **2002**, *106*, 10649.

(29) Wirz, R.; Bürgi, T.; Baiker, A. *Langmuir* **2003**, *19*, 785.

(30) Wirz, R.; Bürgi, T.; Lindner, W.; Baiker, A. *Anal. Chem.* **2004**, *76*, 5319.

(31) Hepel, M.; Tewksbury, E. *J. Electroanal. Chem.* **2003**, *552*, 291.

(32) Takehara, K.; Aihara, M.; Ueda, N. *Electroanalysis* **1994**, *6*, 1083.

(33) Fang, C.; Zhou, X. *Electroanalysis* **2003**, *15*, 1632.

(34) Bieri, M.; Bürgi, T. *Langmuir* **2005**, *21*, 1354.

(35) Urakawa, A.; Wirz, R.; Bürgi, T.; Baiker, A. *J. Phys. Chem. B* **2003**, *107*, 13061.

(36) Becke, A. D. *J. Chem. Phys.* **1993**, *98*, 5648.

(37) Perdew, J. P.; Chevary, J. A.; Vosko, S. H.; Jackson, K. A.; Pederson, M. R.; Singh, D. J.; Fiolhais, C. *Phys. Rev. B* **1992**, *46*, 6671.

(38) Ditchfield, R.; Hehre, W. J.; Pople, J. A. *J. Chem. Phys.* **1971**, *54*, 724.

(39) Frisch, M. J.; Trucks, G. W.; Schlegel, H. B.; Scuseria, G. E.; Robb, M. A.; Cheeseman, J. R.; Montgomery, Jr., J. A.; Vreven, T.; Kudin, K. N.; Burant, J. C.; Millam, J. M.; Iyengar, S. S.; Tomasi, J.; Barone, V.; Mennucci, B.; Cossi, M.; Scalmani, G.; Rega, N.; Petersson, G. A.; Nakatsuji, H.; Hada, M.; Ehara, M.; Toyota, K.; Fukuda, R.; Hasegawa, J.; Ishida, M.; Nakajima, T.; Honda, Y.; Kitao, O.; Nakai, H.; Klene, M.; Li, X.; Knox, J. E.; Hratchian, H. P.; Cross, J. B.; Bakken, V.; Adamo, C.; Jaramillo, J.; Gomperts, R.; Stratmann, R. E.; Yazyev, O.; Austin, A. J.; Cammi, R.; Pomelli, C.; Ochterski, J. W.; Ayala, P. Y.; Morokuma, K.; Voth, G. A.; Salvador, P.; Dannenberg, J. J.; Zakrzewski, V. G.; Dapprich, S.; Daniels, A. D.; Strain, M. C.; Farkas, O.; Malick, D. K.; Rabuck, A. D.; Raghavachari, K.; Foresman, J. B.; Ortiz, J. V.; Cui, Q.; Baboul, A. G.; Clifford, S.; Cioslowski, J.; Stefanov, B. B.; Liu, G.; Liashenko, A.; Piskorz, P.; Komaromi, I.; Martin, R. L.; Fox, D. J.; Keith, T.; Al-Laham, M. A.; Peng, C. Y.; Nanayakkara, A.; Challacombe, M.; Gill, P. M. W.; Johnson, B.; Chen, W.; Wong, M. W.; Gonzalez, C.; Pople, J. A. *Gaussian 03*, Revision C.01; Gaussian, Inc., Wallingford CT, 2004.

(40) Cancès, M. T.; Mennucci, B.; Tomasi, J. *J. Chem. Phys.* **1997**, *107*, 3032.

(41) Bird, R. B.; Stewart, W. E.; Lightfoot, E. N. *Transport Phenomena*; John Wiley & Sons: New York, 1960.

(42) *FEMLAB*, v.3.0; COMSOL, Inc.: Stockholm, Sweden.

(43) Pintar, A.; Malacea, R.; Pinel, C.; Fogassy, G.; Besson, M. *Appl. Catal., A* **2004**, *264*, 1.

(44) Osawa, M.; Ataka, K.-I.; Yoshii, K.; Nishikawa, Y. *Appl. Spectrosc.* **1993**, *47*, 1497.

(45) Wadayama, T.; Sakurai, T.; Ichikawa, S.; Suëtaka, W. *Surf. Sci.* **1988**, *198*, L359.